Surface chemistry controls the density of states in metallic nanoparticles

Nicholas P. Litak, Lillian M. Mawby, and Benjamin J. Lear*

Department of Chemistry, The Pennsylvania State University, University Park, PA 16802, United States of America

E-mail: bul14@psu.edu

Phone: +1 814-867-4625

Abstract

Ligand-stabilized colloidal metallic nanoparticles are prized in science and technology for their electronic properties and tunable surface chemistry. However, little is known about the interplay between these two aspects of the particles. A particularly glaring absence concerns the density of electronic states, which is fundamental in explaining the electronic properties of solid-state materials. In part, this absence owes to the difficulty in the experimental determination of the parameter for colloidal systems. Herein, we demonstrate the density of electronic states for metallic colloidal particles can be determined from their magnetic susceptibility, measured using nuclear magnetic resonance spectroscopy. For this study, we use small alkanethiolate protected gold nanoparticles and demonstrate that changes in the surface chemistry, as subtle as changes in alkane chain length, can result in as much as a three-fold change in the density of states at the Fermi level for these particles. This suggests that surface chemistry can be a powerful tool for controlling the electronic behavior of the materials to which they are attached, and suggests a paradigm that could be applied to other metallic systems, such as other metal nanoparticles, doped semiconductor systems, and even

2D metals. For all of these metallic systems, the Evans method can serve as a simple means to probe the density of states near the Fermi level.

Keywords

gold, nanoparticles, ligands, NMR, magnetic susceptibility, density of states, electronic bands

Ligand-stabilized metallic nanoparticles are a fixture of modern science, enabling applications that include advanced spectroscopy, sensors, cancer treatments, and catalytic transformations.[1–7] There are two reasons for this ubiquity. First, these particles possess unique electronic properties which can be tuned—most commonly through *physical* changes to the metallic core's size and shape.[8] Equally important are the particles' tunable surface chemistry, which enables their dispersion within a wide range of aqueous and non-aqueous environments. Despite the importance of both these properties, and the fact that ligand control over metal centers is the dominant paradigm in molecular inorganic chemistry,[9] relatively little is known about how surface *chemistry* may be used to control the electronic properties of the metallic core of nanoparticles. Particularly striking is the absence of discussion regarding how surface chemistry can influence the density of electronic states at the Fermi energy, $g(E_F)$, which is a fundamental parameter for describing metals in solid-state physics. In part, this absence is due to difficulty in measuring $g(E_F)$ for the colloidal systems of interest. Here, we introduce a method for measuring $g(E_F)$ for colloidal nanoparticles and then report $g(E_F)$ for nanoparticles protected with a series of alkanethiols. We observe that these subtle chemical changes exert a strong influence over the density of states and that this influence is fundamentally different from that attainable by physical changes. Thus, our work suggests the rational use of surface chemistry could produce additional, finely tuned behaviors in these ubiquitous nanoparticles. Furthermore, our findings should be applicable to other *metallic* nanoscale systems, such as doped semiconductor nanoparticles and 2D metals.

Importantly, the current lack of research connecting surface chemistry to $g(E_F)$ is not due to a lack of interest, as $g(E_F)$ is known to control behaviors such as electronic and thermal conductivity[10] as well as catalytic activity.[11] Instead, the knowledge gap is a result of difficulties in applying conventional methods for measuring $g(E_F)$ to colloidal systems. Techniques such as x-ray photoemission spectroscopy,[12] angle-resolved photoemission spectroscopy,[13] and x-ray magnetic circular dichroism[14] require high vacuum conditions that

preclude the use of the solvents inherent to colloidal suspensions. At the same time, the organic ligands that enable widespread use of the nanoparticles are insulating and can lead to charging effects that complicate the use of measurements based on scanning probe[15] electron microscopy,[16] and photoemission.[12,13] This is particularly problematic when changing ligands, which could confuse changes in these charging effects with changes in electronic structure. Moreover, all of these techniques convolve high energy electronic states in the measurement, complicating unambiguous isolation of the ground state $g(E_F)$.

Herein, we demonstrate an NMR-based measurement of Pauli paramagnetism that allows the determination of $g(E_F)$ while avoiding all of the above complications (Figure 1). Pauli paramagnetism arises from the partially-filled electronic band that is a defining characteristic of metallic systems. Figure 1 depicts generalized α and β spin bands, drawn with the commonly assumed Gaussian profile. Application of a magnetic field produces Zeeman splitting of the spin bands and electrons are then transferred to maintain a constant Fermi energy, E_F. The number of electrons transferred, and associated volumetric Pauli paramagnetic susceptibility, χ_{vol}^{Pauli}, is directly related to $g(E_F)$ by:[17]

$$\chi^{Pauli} = \mu_0 \mu_B^2 g(E_F) \tag{1}$$

where μ_0 is the permeability of free space and μ_B is the Bohr magneton. It is important to note that this treatment assumes only a partially filled electronic band, and does not consider the band's identity.

Our interest in ligand control of $g(E_F)$ was inspired by the long-standing work of Ulman and co-workers, who reported the surface potential (directly related to E_F) of gold under a series of self-assembled monolayers of alkanethiols with different lengths. They found the surface potential increased at a linear rate of 9.3 meV per methylene unit.[18] We noticed this result correlated well with the calculated ionization potential of alkanethiols, IP_{calc}^{ligand} (Table 1),[19] suggesting these same ligands might also be used to adjust the energy of E_F in colloidal

metallic nanoparticles. A brief consideration of the structure of electronic bands (Figure 1) will show that increasing E_F will produce a change in $g(E_F)$. Indeed, if alkanethiols were to exert the same control for nanoparticles as for bulk gold, then moving from butanethiol to dodecanethiol could adjust $g(E_F)$ by as much as 3-fold[11,20] and this effect should be observable as a concomitant change in Pauli paramagnetic susceptibility (Equation 1).

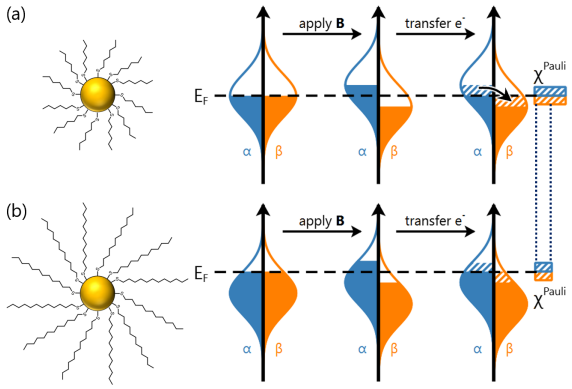

Figure 1: Graphical depiction of the hypothesis guiding the work. Pauli paramagnetism arises for metals placed in a magnetic field, where Zeeman splitting lifts the degeneracy of the α and β spin bands, leading to the transfer of electrons between bands to preserve a constant Fermi level. The excess electron population in one spin manifold produced by this transfer produces the Pauli paramagnetism. This behavior is expected of any metallic system and so we leave the bands drawn as unidentified, generic, bands. Germane to this paper: the magnitude of the Pauli paramagnetic susceptibility, χ^{Pauli}, of a metallic system, depends on the position of E_F within the electronic band structure, which we hypothesized might be influenced by surface chemistry. (a) If the Fermi level resides at a region of high density of states, this will produce a larger magnetism than if (b) the Fermi level resides at a region of low density of states. Thus, the observed χ^{Pauli} functions as a probe of the density of electronic states and can be used to follow the influence of surface chemistry. In this figure, the surface chemistry is not drawn to be accurate, but to allow easy comparison of differences in ligand length.

Results/Discussion

To test the hypothesis outlined in the introduction, we synthesized a series of AuNPs bearing alkanethiols with even-numbered carbon chains, from butane to dodecane, following a modified Brust method,[21] and then measured the magnetic susceptibility for each particle set.

For each ligand, we synthesized two batches, for a total of twelve independently synthesized particles. The σ-electron donor strength of these ligands increases with increasing ligand length, as reflected by their calculated ionization potential in hexane (IP^{ligand}, Table 1), which should function to adjust E_F. Figure 2 shows a schematic representation of a particle, the spread of diameters determined using TEM, thermogravimetric analysis (TGA), and their UV-vis spectra for all twelve particles. Table 1 reports the mean diameter and standard deviation obtained from fits of log-normal functions to the distributions of diameters. Exemplars of the micrographs analyzed to yield these distributions, as well as histograms of the diameters and the log-normal fits to these histograms, are shown in the SI. The mean particle sizes we obtain are all between 2.5 nm and 5.0 nm, with a mix of both broad and narrow distributions. Additionally, some of the particles are far from spherical, while others approach spherical. This spread in particle shapes and distributions highlights a particular advantage of the approach outlined below: that neither particle size nor shape is explicitly involved in the analysis. Though size and shape may very well exert control of the electronic properties, we do not *require* tight control over these parameters to perform our analysis. While this means that the population will be represented by a single value and that potential effects of size and shape across a distribution will be obscured, the analysis below will show striking success across all twelve particle samples. This result demonstrates our approach should be applicable to the messy systems common in practical nanoscience and highlights the potential power of ligands for controlling the electronic structure of colloidal metallic nanoparticles.

Though neither size nor shape of the particles is involved in our analysis of Pauli-paramagnetism that follows, in order to maximize the ligand influence, we targeted particles that were small, while remaining within the metallic regime.[22] However, as shown in Figure 2d, this maximized ligand influence comes at the expense of a prominent plasmonic feature. Even for particles with the broadest distributions that extend to large sizes, the plasmonic feature is not strong. However, the lack of plasmon does not pose a problem for our analysis,

nor is the plasmon an ideal probe of the electronic structure of the core, which is the focus of our measurements. Though plasmon resonances are arguably the current dominant tool for investigating electronic behaviors of nanoscale metals, they can experience changes in position and intensity, even in the absence of changes to the electronic structure of the core, and so are not a selective tool for measurement of this property of the particles. Instead, we seek to use measurements of χ^{Pauli}, which is selective for electronic structure (Equation 1), and only requires the particle be metallic. Though our particles display a strongly damped plasmon, the particles we obtained are large enough to place them firmly within the metallic regime,[22] rendering Equation 1 valid.

We measured the magnetic susceptibility of our particles using the Evans NMR method (Figure 3),[23] modified in order to allow resolution of the small susceptibilities expected for our systems. Our variation remains a differential measurement, utilizing two measurements made with coaxial NMR tubes. A thorough description of the technique is provided in the SI, but the basics of the approach are outlined here. In both measurements, the inner tube contained $CDCl_3$, spiked with $CHCl_3$. For the first measurement, the outer tube contained pure hexanes (Figure 3a). For the second measurement, the outer tube contained a suspension of nanoparticles in hexanes (Figure 3b). The presence of the nanoparticles alters the magnetic field within the outer tube, producing a shift in the resonance position of the hexanes that is measured in reference to the inner tube's $CHCl_3$. In our measurements, this shift occurred without a broadening of the NMR line shapes (Figure 3c). The shifts we observe from these measurements are recorded in Table 1, in terms of ppm shift per unit concentration (g/mL) of the nanoparticles, or Δppm_{mass}.

There are two things to note from these measurements. First, the value of Δppm_{mass} depends on ligand identity. Second, the shifts we observe are in the direction of lower ppm, indicating that the overall magnetic response upon adding nanoparticles to our solvent is diamagnetic, and the susceptibility associated with our measurement is negative. We can

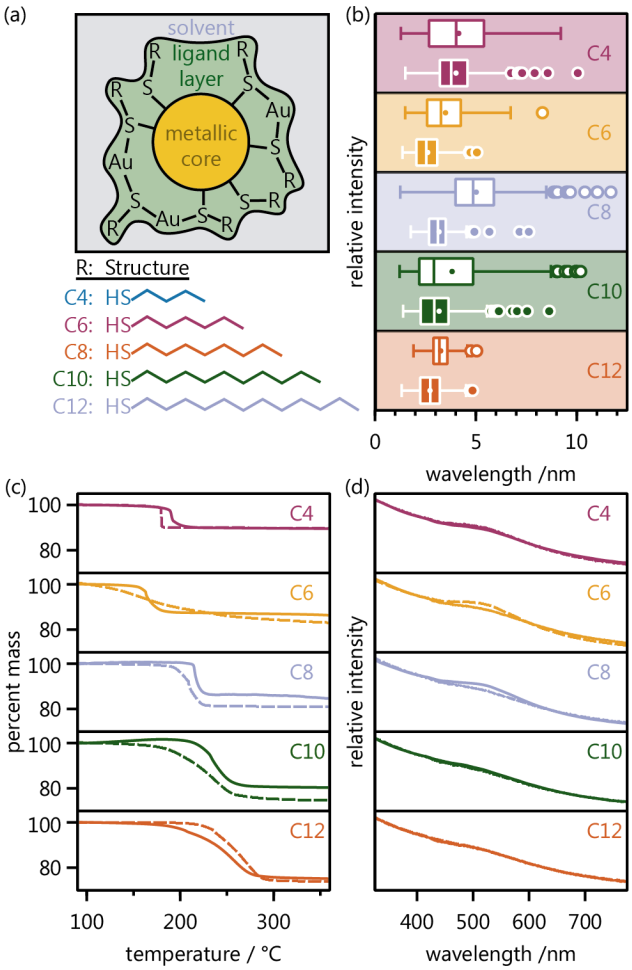

Figure 2: A summary of the chemical structure and physical properties of the nanoparticles. (a) The colloidal nanoparticle system can be divided into the solvent, ligand shell, and metal core. The alkanethiols we use for this study are known to bind to the metal core in a large number of possible arrangements, and this cartoon depicts a few of these arrangements. (b) Box and whisker plots of the diameters for the metal core of all nanoparticles reported in this manuscript, as measured from TEM. In this figure, the box encloses the interquartile range (IQR), the median diameter is indicated by the vertical line within the box, the arithmetic mean is indicated by the small dot in the box, the whiskers extend to 1.5 the IQR, and outliers beyond the whiskers are drawn with circles. For each ligand, two batches of nanoparticles were synthesized, one batch is represented with colored lines on the box, while the other is represented with white lines on the box. Geometric means and standard deviations are also obtained for these particles by fitting log-normal function distribution to the distributions. These values are given in Table 1. (c) Curves obtained from thermal gravimetric analysis showing the temperatures associated with ligand loss. The percent mass loss allows the determination of the relative masses of the ligand shell and metal core, as summarized in Table 1. Here, solid curves correspond to the same particles that were represented by the box and whisker plots with colors lines. (d) UV-visible spectra of the particles in hexanes, each normalized to the intensity at 400 nm. Each spectrum shows a strongly damped plasmonic feature. Again, solid lines correspond to the same particles that yielded the solid curves for TGA as well as the box and whisker plots with colored outlines on the boxes.

convert Δppm_{mass} to an observed mass susceptibility, χ^{obs}_{mass}, using:[23]

$$\chi^{obs}_{mass} = \frac{3\Delta\text{ppm}_{mass}}{4\pi 10^6} \tag{2}$$

The resulting χ^{obs}_{mass} are plotted in Figure 3d and recorded in Table S5

Perhaps the most striking feature of Figure 3d is the non-monotonic nature of the data. This, in part, reflects the trends in sizes of the particles and the trend in the fractional mass of the ligands, each of which contributes their own magnetic behaviors beyond the Pauli paramagnetism of interest. In fact, we find it convenient to decompose the value of χ^{obs}_{mass} into a linear combination of five magnetic susceptibilities:

$$\chi^{obs} = \chi^{Pauli} + \chi^{Landau} + \chi^{core} + \chi^{shell} - \chi^{solvent} \tag{3}$$

from which χ^{Pauli} can be isolated. These susceptibilities are:[17]

χ^{Pauli}: resulting from Zeeman splitting of the partially filled electronic band (Figure 1), this contribution is paramagnetic

χ^{Landau}: classically, this is explained by Lenz's law, whereby mobile electrons placed in a magnetic field will produce a ring current, with a magnetic moment that opposes the applied field (diamagnetic). Though this is not active for particles of our size, there are quantum-mechanical orbital effects that can also produce diamagnetism and are also termed Landau magnetism

χ^{core}: in addition to the conduction electrons, each gold atom possesses filled core orbitals (1s through 5d), whose contributions are diamagnetic

χ^{shell}: the core is surrounded by a ligand 'shell,' composed of atoms with complete electronic shells, yielding a contribution that is diamagnetic

$\chi^{solvent}$: this contribution to Equation 3 is negative because the solvent is displaced by the nanoparticle. We used hexanes as our solvent, which is diamagnetic

Notably absent from Equation 3 is any contribution from isolated paramagnetism on the nanoparticles. Despite many intriguing examples of paramagnetism in AuNPs in the literature,[24] isolated paramagnetism is not uniformly observed for gold nanoparticles, and so we must verify that its absence from Equation 3 is warranted in our case.

Initial evidence for the lack of any significant contribution from isolated paramagnetism is the simple fact that the overall behavior of our particles is diamagnetic. The susceptibility of isolated paramagnetic centers is several orders of magnitude stronger than any of the other contributions discussed above.[17] Thus, if isolated paramagnetism was present, the net response should be paramagnetic. However, stronger evidence is found in the temperature dependence of our samples. The diamagnetic contributions from χ^{core}, χ^{shell}, and $\chi^{solvent}$ are expected to be nearly temperature independent.[17] Though χ^{Pauli} for a free electron gas is often treated as temperature-independent, real metals can show *direct* temperature dependence, due to expansion of the metal lattice with increasing temperature. The increased distance between metal atoms decreases the electronic coupling and the associated band dispersion. As a result, $g(E_F)$ and χ^{Pauli} increase with temperature.[25] On the other hand, isolated paramagnetism follows Curie-Weiss behavior, with χ decreasing with increasing temperature.[17] and, though real metals can also show such inverse temperature dependencies, they are much weaker than for isolated paramagnetic systems.

This last point is not actually needed, as Figure 3e shows that our hexanethiol nanoparticles in THF possess a *direct* temperature dependence of χ^{obs}_{mass} over the range 180 K to 250 K in THF. THF was used, as opposed to hexanes, in order to provide access to lower temperatures in the liquid state. The plotted values can be found in Table S1. The increasing paramagnetism (more positive χ^{obs}) with increasing temperature not only indicates that isolated paramagnetism *cannot* be a dominant contributor to χ^{obs}, but also that χ^{Pauli} must be the dominant source of paramagnetism in our system.

We are now ready to isolate χ^{Pauli} by determining the value of each other term in Equation 3. The SI provides a detailed walk-through of our method, but we can summarize the

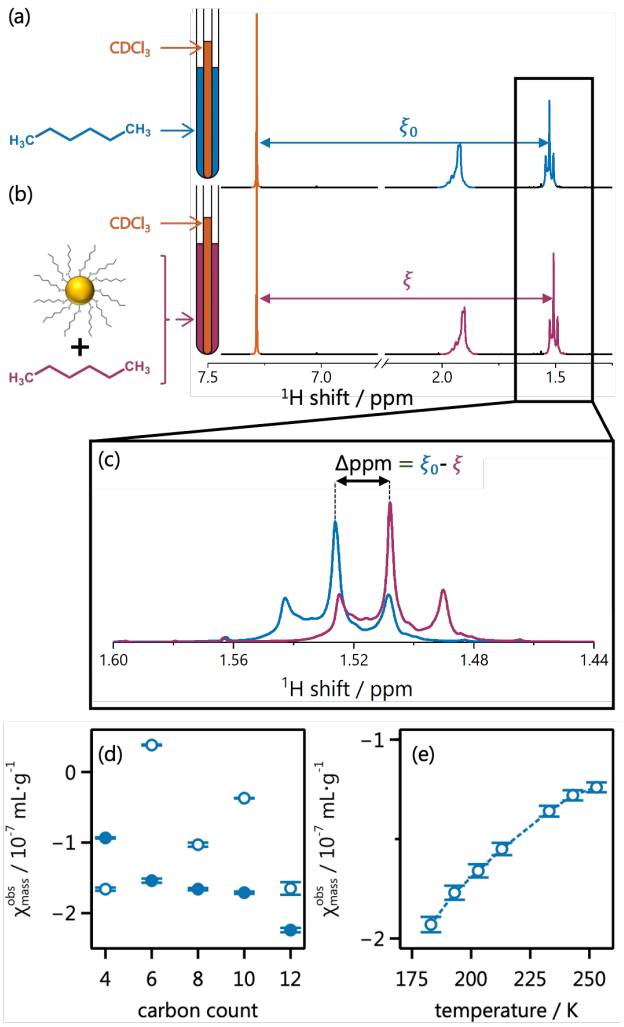

Figure 3: Measurements of the magnetic properties were performed using the Evans method of NMR. (a) First, an NMR spectrum is taken using a pair of coaxial NMR tubes, in which the inner tube contains $CDCl_3$ and the outer tube has pure hexanes. For visual clarity, we illustrate this for *n*-hexane. (b) Next, a new outer tube is used which contains a colloidal suspension of nanoparticles in hexanes, and a new spectrum acquired. (c) The difference in chemical shift, relative to the chloroform in the inner tube, is determined and Equation 2 is used to convert this shift to χ_{mass}^{obs}. (d) A plot of χ_{mass}^{obs} for our AuNPs in hexanes, as a function of carbon count. Here, filled markers correspond to the particles represented by the solid lines and box and whisker plots with colored outlines in Figure 2. (e) Temperature dependence of χ_{mass}^{obs} for nanoparticles protected with hexanethiol in THF. THF was used to provide access to lower temperatures in the liquid state, as compared to hexanes. The error bars represent the propagation of the errors in concentration.

overall approach here. First, we use the fact that χ^{Landau} is directly related to χ^{Pauli} via:[17]

$$\chi^{Pauli} = -3\left(\frac{m^*}{m_e}\right)^2 \chi^{Landau} \tag{4}$$

where m_e is the mass of a free electron and m^* is the effective mass of an electron in the metal. Though this may not be quantitatively accurate for our samples (for instance, χ^{Landau} could be close to zero), we do not think that its value will change dramatically from sample to sample, and so the observed relative *differences* between samples are valid, while the mean value about which they change could be shifted by assuming a different Landau magnetism (see below). Given the size of our particles, we assume that the effective mass is the same as for bulk gold ($m^* = 1.1m_e$).[26] The appropriateness of this approximation, as well as of the other approximations we use, is discussed in the SI. Next, χ^{core} is estimated from the experimentally determined diamagnetic component of bulk gold,[27] weighted by the relative mass of gold in the nanoparticle. This relative mass is obtained by thermal gravimetric analysis shown in Figure 2c and reported in Table 1. Similarly, χ^{shell} is obtained by weighting the susceptibility of the pure ligands by the relative mass of the shell. Finally, we use a literature value[28] for $\chi^{solvent}$ and assume that the volume of solvent displaced equals the nanoparticle volume. It is important to note that neither the gold core size nor particle shape enters into any of these calculations.

The values of χ^{Pauli} obtained from this analysis are given in Table 1, and plotted in Figure 4 against the calculated energy of the ligand ground state with respect to that of butanethiol ($IP^{butanethiol} - IP^{ligand}$).[19] Increasing the energy of the ligand ground state is accompanied by a decrease in χ^{Pauli}. For reference, the value of χ^{Pauli} for bulk gold is also indicated by the dashed grey line.

Remembering that these particles are well within the metallic regime, the similarity of our χ^{Pauli} to that of bulk gold is satisfying. The fact that some of our χ^{Pauli} values are larger for our particles than for bulk gold could indicate a property unique to these nanoscale systems,

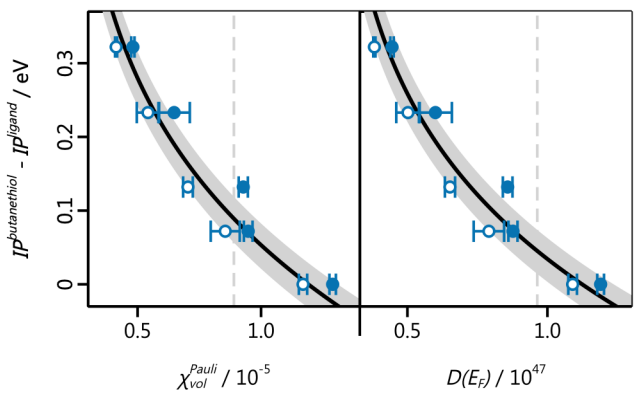

Figure 4: Plots of the dependence of magnetic and electronic properties on surface chemistry for gold nanoparticles. (left) Plot of χ_{vol}^{Pauli}, versus the energy of the ligand ground electronic state. (right) Plot of $g(E_F)$, versus the energy of the ligand ground electronic state. In both cases, the value of the property for bulk gold is shown as a dashed grey line and the energy of the ligand ground state is with reference to that of butanethiol. Also shown as the solid black line is a fit of our data using the Gaussian distribution shown for the density of states in Figure 1. The error bars presented are the errors associated with each experimental measurement. As discussed in the SI, we estimate that our assumptions made in the analysis could lead to a 10% error in the obtained values. The shaded grey regions about the fit line indicate the region of 10% confidence in fit parameters.

or could be a result of the assumptions and approximations we used, as discussed above and in the SI. For instance, if we instead assumed χ^{Landau} was zero, all of our values for χ^{Pauli} would fall below that of bulk gold. Thus, we feel it is best to focus, not on the absolute values, but the trends in χ^{Pauli}, which show a clear dependence on ligand identity, with the effect being consistent across all particles.

The motivation for our work was using Equation 1 to follow the change in $g(E_F)$ with changes in surface chemistry. The values of $g(E_F)$ obtained from this equation are given in Table 1 and plotted in Figure 4. The closeness to the value for bulk gold is again satisfying, though we offer the same caution regarding the value rising above that of the bulk. However, we wish to draw attention to the clear dependence of $g(E_F)$ on the ligand identity, experiencing a nearly 3-fold change, which is in agreement with the prediction outlined earlier in this manuscript.

This ligand dependence can be explained as follows. Based upon the atomic electronic structure of gold, [Xe] $4f^{14}$ $5d^{10}$ $6s^1$, the partially filled band for *pure* gold is half-filled and,

according to the simplified picture shown in Figure 1a, $g(E_F)$ is at a maximum. Attaching alkanethiol to gold will adjust the E_F of the gold, with longer ligands pushing the E_F up in energy[18,19] and to areas of lower density of states. As depicted in Figure 1, the density of states is expected to have a Gaussian profile with respect to energy. Thus, as E_F moves upward from the halfway point, the measured $g(E_F)$ should follow the sigmoidal-like curve associated with the side of a Gaussian profile. This expectation is verified by the solid black lines in Figure 4, which were generated by fitting a Gaussian function to our data. The need for a non-linear model for fitting this data is verified in the SI.

While it is satisfying that the trends shown in Figure 4 match the expected behavior for changing the energy of the E_F, it is worth noting that these systems are complex, and changes in ligands may also result in changes in ligand structure,[29] surface chemistry,[30] or core symmetry,[22] all of which could produce changes to the DOS. In addition, it is worth acknowledging that all of our particles have different mean diameters and widths of the size distributions. While our analysis does not take into account the sizes, one could reasonably expect that the changes in the surface-area-to-volume ratio that changes as a function of size would affect the strength of the ligand influence over the density of states. This may account for some of the scatter in our data.

Though the above factors could affect our measured values of χ^{Pauli} and $g(E_F)$, none of them are expected to produce the Gaussian-shaped dependence seen in Figure 4. Thus, while it is important to acknowledge these possible contributions to the ligand-induced control exerted over the electronic structure of the metallic core, we propose that the ligand-induced change in E_F through a Gaussian-shaped electronic band is the most likely explanation of our observed non-linear trend. Nevertheless, we stress that the primary focus of this work is not an establishment of the *mechanism* of action, but the demonstration of dramatic ligand influence over the density of states in metallic systems and the ability to clearly measure it. We hope that subsequent work will allow elucidation of a clear mechanism of action.

With regard to the ability to make these measurements, the NMR approach demon-

strated here provides a much more sensitive probe of changes in the electronic structure of these particles than does the UV-vis spectrum. The SI provides an analysis of the nascent plasmonic features seen in Figure 2d. In particular, the position of the plasmon, often used as a gauge of changes in particle behavior, shows no strong trend with ligand length. The lower sensitivity of the plasmonic feature to changes in $g(E_F)$, as compared to the NMR-based approach, could be a result of the weakness of the features in our particles, a lack of selectivity for probing electronic structure, the relative breadth of the plasmon bands, or some combination of these limitations. However, this study does show the advantages of using NMR to probe the electronic structure of metallic systems and highlights the applicability to a wide range of metallic systems, many of which may not exhibit strong plasmonic features.

It is also particularly noteworthy that the nearly 3-fold change in $g(E_F)$ that we observe is *not* accessible by the physical changes that currently dominate attempts to tune the electronic behaviors of nanoscale metals. At diameters significantly larger than the metallic threshold, and in the absence of environmental effects, a metallic core will have a $g(E_F)$ near that of the bulk, no matter changes in size and shape. Thus, our results demonstrate that the tunability offered by surface chemistry complements and extends the tunability provided by physical means and should be applicable to other metallic systems. More importantly, the large change to the electronic structure we have demonstrated here was accomplished using alkanethiols. These ligands are by no means optimal for exerting influence over gold, and the conceptual frameworks and ligands developed by molecular inorganic chemists over the past century[9] should provide fertile ground for exploration.

Finally, we wish to reiterate that the approach to measuring the density of states is expected to be applicable in general for metallic systems. These include colloidal metal nanoparticle systems that lie in the same size-regime, or larger, as those we have reported on here. Indeed, the fundamental requirement for our analysis is that the systems under consideration have no appreciable band-gap so that they exhibit Pauli-paramagnetism. This

is a property that is shared not only by other metal nanoparticles but by a diverse and growing array of materials, such as 2D metals and doped semiconductors. All of these systems should fall under the purview of the technique we have demonstrated above, though sample preparation may prove challenging in some cases.

We also expect that ligand control over metallic properties should be similarly general. Though the precise response to changes in ligands may vary from system to system, in all cases the binding of ligands to metal interfaces is a chemical event that should perturb the electronic states within the metal and which will allow chemical control over the properties of metals. Given the diverse array of ligand available, a proper understanding of ligand design and effects will provide us a precisely tunable means of controlling the electronic behaviors of metallic systems, including metal nanoparticles, 2D metals, and doped semiconductors.

Conclusions

Using the Evans method of NMR, we measured the magnetic susceptibility of small metallic gold nanoparticles protected with alkanethiolate ligands. We then demonstrated that this susceptibility changed with the chain length of the alkane and that, in particular, the Pauli paramagnetism of the metallic core is inversely proportional to the length of the alkane chain. Because it is known that increasing the chain length of alkanethioates will increase the energy of the HOMO of the sulfur atom, we postulate that increasing chain length causes more charge donation across the Au-S bond, which pushes the Fermi energy higher in the electronic band structure and to regions of lower density of electronic states. It is the movement of the Fermi energy to regions of lower density of electronic states that gives rise to the observed reduction in the magnetic susceptibility. Taken as a whole, this work demonstrates that ligands can be used to rationally tune the electronic structure of metallic systems to which they are attached.

Methods/Experimental

Nanoparticle synthesis

The AuNPs used in this study were prepared using a modified two-phase Brust method[21] with a $HAuCl_4 \cdot 3H_2O$ to alkanethiol molar ratio of 1.0: 1.83. $HAuCl_4 \cdot 3H_2O$ (180 mg, 0.46 mmol) was dissolved in 30 mL of deionized H_2O. To the aqueous gold solution, tetraoctyammonium bromide (1.09 g, 2.00 mmol), dissolved in toluene (20 mL), was added. The mixture was stirred until the transfer of gold to the organic layer was complete. Phase transfer completion was indicated by the emergence of an interface between the aqueous and organic layers, and the transition of the aqueous layer from red/orange to colorless.

The aqueous layer was discarded. Alkanethiol (0.84 mmol) was added to the organic layer via syringe, and the mixture immediately transitioned in color from red-orange to cloudy white. $NaBH_4$ (180 mg, 4.8 mmol) dissolved in deionized H_2O was added in a drop-wise manner. The mixture changed in color from cloudy white to black. The gold-alkanethiol mixture stirred for 3 hours. The aqueous layer was discarded and 250 mL of MeOH was added to the organic layer. The mixture was placed in the freezer overnight (or for at least 10 hours).

The particles precipitated out of solution after 10 hours. The precipitate was collected over a fritted filter and suspended in toluene. AuNPs in 1:19 toluene to methanol (MeOH) solution were centrifuged for 15 min at 10,000 RPM. This washing process was repeated twice using the same toluene – MeOH ratio. Finally, the AuNPs were collected with tetrahydrofuran (THF) and dried via a rotary evaporator. Final yields ranged between 95.1 and 131.5 mg per synthesis.

Thermograviemtric analysis (TGA) preparation

"Dry" AuNPs (especially those capped with longer alkanethiols), were found to be quite waxy and difficult to place on TGA pans. To overcome this difficulty, the particles were

molded into a "pellet" via centrifugation.

Similar to the washing method (see above), AuNPs suspended in toluene were placed in centrifuge tubes. MeOH was added until the volumetric ratio of toluene to MeOH came to be 1:19. The tubes were run through one cycle in the centrifuge at 10,000 RPM for 15 min. The supernatant was decanted and the "pellet" collected.

Instrumentation

Transmission electron microscopy (TEM) images were collected using an FEI Tecnai G2 20 XTWIN microscope with a LaB6 source operating at 200 kV. All Evans measurements were performed using a Bruker AV-III-HD-500 MHz nuclear magnetic resonance spectrometer. TGA measurements were performed using TA Instruments Discovery Series TGA Q5500 coupled with Discovery MS. Samples were heated from room temperature to 700 °C at a rate of 20 °C/min under N_2 atmosphere using a high-temperature platinum pan.

Data availability

All data used in this report are found in the main manuscript and the supplemental information. Raw NMR, TGA, and TEM data are available upon request.

Supporting Information Available

Tables of temperature-dependent data, all parameters used in calculation of χ^{Pauli}, description of the Evans method, detailed walkthrough of the calculation of χ^{Pauli}, and discussion of the assumptions used can be found free of charge in the online supplemental information.

Author contributions

All authors were involved in the design of experiments, the analysis of data, and the writing and editing of this manuscript. NL and LM were also involved in the collection of the data.

Competing interests

The authors declare no competing interests in this work.

Acknowledgement

The authors acknowledge the NSF (CHE-1609572 and CHE-2003609) for financial support. NPL acknowledges Penn State's Erickson Discovery Grant for support. BJL acknowledges the Fulbright Finland Foundation for support during the writing of the manuscript.

Table 1: Calculated and measured parameters of the nanoparticles. Reported here are the calculated ionization potential of the isolated ligand, the measured mean core diameter and associated standard deviation, the measured ligand to core mass ratio, the measured NMR Evans shift, normalized by the mass concentration of the particles, the volumetric Pauli paramagnetism determined using Equation 3, and the density of states associated with the Pauli paramagnetism, as determined from Equation 1. Errors for the Δppm_{mass} come from fits of the experimental data. The remaining errors come from propagating the experimental errors during calculations.

ligand	IP_{Ligand}	Batch	d^{core} / nm	σ_d^{core} / nm	$\frac{m_{shell}}{m_{core}}$	Δppm_{conc} / mL·g^{-1}	χ_{vol}^{Pauli} / 10^{-5}	$g(E_F)$ / $10^{47}\text{J}^{-1}\cdot\text{m}^{-3}$
1-butanethiol	7.776	A	4.13 ± 0.35	1.78 ± 0.015	0.109	-0.391 ± 0.004	1.285 ± 0.013	1.190 ± 0.012
		B	3.75 ± 0.04	1.29 ± 0.01	0.115	-0.698 ± 0.010	1.174 ± 0.017	1.087 ± 0.016
1-hexanethiol	7.704	A	3.26 ± 0.08	1.48 ± 0.03	0.153	-0.648 ± 0.012	0.948 ± 0.018	0.878 ± 0.016
		B	2.50 ± 0.05	1.37 ± 0.03	0.193	-0.160 ± 0.011	0.855 ± 0.059	0.791 ± 0.054
1-octainethiol	7.644	A	5.00 ± 0.16	1.32 ± 0.04	0.157	-0.697 ± 0.007	0.928 ± 0.019	0.859 ± 0.017
		B	3.11 ± 0.04	1.23 ± 0.01	0.223	-0.432 ± 0.012	0.704 ± 0.020	0.652 ± 0.018
1-decanethiol	7.543	A	2.64 ± 0.12	1.40 ± 0.06	0.242	-0.715 ± 0.007	0.648 ± 0.064	0.600 ± 0.059
		B	2.86 ± 0.09	1.41 ± 0.04	0.445	-0.156 ± 0.013	0.542 ± 0.045	0.502 ± 0.042
1-dodecanethiol	7.454	A	3.20 ± 0.05	1.16 ± 0.02	0.325	-0.941 ± 0.013	0.481 ± 0.007	0.445 ± 0.006
		B	2.75 ± 0.06	1.32 ± 0.03	0.406	-0.689 ± 0.007	0.413 ± 0.004	0.382 ± 0.004

References

(1) Peng, F.; Setyawati, M. I.; Tee, J. K.; Ding, X.; Wang, J.; Nga, M. E.; Ho, H. K.; Leong, D. T. Nanoparticles promote in vivo breast cancer cell intravasation and extravasation by inducing endothelial leakiness. *Nature Nanotechnology* **2019**, *14*, 279–286.

(2) Xiong, L.; Sun, Z.; Zhang, X.; Zhao, L.; Huang, P.; Chen, X.; Jin, H.; Sun, H.; Lian, Y.; Deng, Z.; Rümmerli, M. H.; Yin, W.; Zhang, D.; Wang, S.; Peng, Y. Octahedral gold-silver nanoframes with rich crystalline defects for efficient methanol oxidation manifesting a CO-promoting effect. *Nature Communications* **2019**, *10*, 3782.

(3) Plech, A.; Kotaidis, V.; Lorenc, M.; Boneberg, J. Femtosecond laser near-field ablation from gold nanoparticles. *Nature Physics* **2006**, *2*, 44–47.

(4) Zhang, J.; Wang, L.; Zhang, B.; Zhao, H.; Kolb, U.; Zhu, Y.; Liu, L.; Han, Y.; Wang, G.; Wang, C.; Su, D. S.; Gates, B. C.; Xiao, F.-S. Sinter-resistant metal nanoparticle catalysts achieved by immobilization within zeolite crystals via seed-directed growth. *Nature Catalysis* **2018**, *1*, 540–546.

(5) Zhan, C.; Chen, X.-J.; Yi, J.; Li, J.-F.; Wu, D.-Y.; Tian, Z.-Q. From plasmon-enhanced molecular spectroscopy to plasmon-mediated chemical reactions. *Nature Reviews Chemistry* **2018**, *2*, 216–230.

(6) Lee, H.-E.; Ahn, H.-Y.; Mun, J.; Lee, Y. Y.; Kim, M.; Cho, N. H.; Chang, K.; Kim, W. S.; Rho, J.; Nam, K. T. Amino-acid- and peptide-directed synthesis of chiral plasmonic gold nanoparticles. *Nature* **2018**, *556*, 360–365.

(7) Kang, H.; Kang, H.; Buchman, J. T.; Rodriguez, R. S.; Ring, H. L.; He, J.; Bantz, K. C.; Haynes, C. L. Stabilization of Silver and Gold Nanoparticles: Preservation and Improvement of Plasmonic Functionalities. *Chemical Reviews* **2019**, *119*, 664–669.

(8) Willets, K. A.; Duyne, R. P. V. Localized Surface Plasmon Resonance Spectroscopy and Sensing. *Annual Review of Physical Chemistry* **2007**, *58*, 267–297.

(9) Cotton, F. A.; Wilkinson, G. *Advanced Inorganic Chemistry*; Wiley: New York, New York, 1962.

(10) Simon, S. H. *The Oxford Solid State Basics*; Oxford University Press: Oxford, UK, 2013.

(11) Carchini, G.; Almora-Barrios, N.; Revilla-Lopez, G.; Bellarosa, L.; Garcıa-Muelas, R.; Garcıa-Melchor, M.; Pogodin, S.; Błonski, P.; Lopez, N. How Theoretical Simulations Can Address the Structure and Activity of Nanoparticles. *Topics in Catalysis* **2013**, *56*, 1262–1272.

(12) Fadley, C. S.; Shirley, D. A. Electronic Density of States from X-Ray Photoelectron Spectroscopy. *Journal of Research of the National Bureau of Standards, A* **1970**, *74A*, 543–558.

(13) Olson, C. G.; Liu, R.; Lynch, D. W.; List, R. S.; Arko, A. J.; Veal, B. W.; Chang, Y. C.; Jiang, P. Z.; Paulikas, A. P. High-resolution angle-resolved photoemission study of the Fermi surface and the normal-state electronic structure of $Bi_2Sr_2CaCu_2O_8$. *Physical Review B* **1990**, *42*, 381.

(14) Antonov, V. N.; Uba, S.; Uba, L. Electronic structure and x-ray magnetic circular dichroism in the hyperhoneycomb iridate β–Li_2IrO_3. *Physical Review B* **2018**, *98*, 245113.

(15) Li, J.; Schneider, W.-D.; Berndt, R. Local density of states from spectroscopic scanning-tunneling-microscope images: Ag(111). *Physical Review B* **1997**, *56*, 7656–7659.

(16) Pardini, L.; Löffler, S.; Biddau, G.; Hambach, R.; Kaiser, U.; Draxl, C.; Schattschneider, P. Mapping Atomic Orbitals with the Transmission Electron Microscope: Images

of Defective Graphene Predicted from First-Principles Theory. *Physical Review Letters* **2016**, *117*, 036801.

(17) Blundell, S. *Magnetism in Condensed Matter*; Oxford University Press: Oxford, UK, 2001.

(18) Evans, S. D.; Ulman, A. Surface potential studies of alkyl-thiol monolayers adsorbed on gold. *Chemical Physics Letters* **1990**, *170*, 462–466.

(19) Cirri, A.; Silakov, A.; Jensen, L.; Lear, B. J. Chain Length and Solvent Control over the Electronic Properties of Alkanethiolate-Protected Gold Nanoparticles at the Molecule-to-Metal Transition. *Journal of the American Chemical Society* **2016**, *138*, 15987–15993.

(20) Malola, S.; Kaappa, S.; Häkkinen, H. Role of Nanocrystal Symmetry in the Crossover Region from Molecular to Metallic Gold Nanoparticles. *The Journal of Physical Chemistry C* **2019**, *123*, 20655–20663.

(21) Brust, M.; Walker, M.; Bethell, D.; Schiffrin, D. J.; Whyman, R. Synthesis of thiol-derivatised gold nanoparticles in a two-phase Liquid-Liquid system. *Journal of the Chemical Society, Chemical Communications* **1994**, 801–802.

(22) Negishi, Y.; Nakazaki, T.; Malola, S.; Takano, S.; Niihori, Y.; Kurashige, W.; Yamazoe, S.; Tsukuda, T.; Häkkinen, H. A Critical Size for Emergence of Nonbulk Electronic and Geometric Structures in Dodecanethiolate-Protected Au Clusters. *Journal of the American Chemical Society* **2015**, *137*, 1206–1212.

(23) Piguet, C. Paramagnetic Susceptibility by NMR: The "Solvent Correction" Removed for Large Paramagnetic Molecules. *Chemical Education* **1997**, *74*, 815.

(24) Nealon, G. L.; Donnio, B.; Greget, R.; Kappler, J.-P.; Terazzi, E.; Gallani, J.-L. Magnetism in gold nanoparticles. *Nanoscale* **2012**, *4*, 5244–5258.

(25) Hurd, C. M. The magnetic susceptibility of silver and gold in the range 6–300K. *Journal of Physics and Chemistry of Solids* **1966**, *27*, 1371–1374.

(26) Kasap, S. *Principles of Electronic Materials and Devices*; McGraw-Hill: New York, New York, 2005.

(27) Sozuki, M.; Kawamura, N.; Miyagawa, H.; Garitaonandia, J. S.; Yamamoto, Y.; Hori, H. Measurement of a Pauli and Orbital Paramagnetic State in Bulk Gold Using X-Ray Magnetic Circular Dichroism Spectroscopy. *Physical Review Letters* **2012**, *108*, 047201.

(28) Rumble, J. *CRC Handbook of Chemistry and Physics, 67th Edition*; CRC Press: Boca Raton, Florida, 1986.

(29) Antonello, S.; Arrigoni, G.; Dainese, T.; Nardi, M. D.; Parisio, G.; Perotti, L.; René, A.; Venzo, A.; ; Maran, F. Electron Transfer through 3D Monolayers on Au_{25} Clusters. *ACS Nano* **2014**, *8*, 2788–2795.

(30) Häkkinen, H. The gold-sulfur interface at the nanoscale. *Nature Chemistry* **2012**, *4*, 443–455.

TOC image